

## **New convex grating types for concentric imaging spectrometers**

P. Mouroulis, D. W. Wilson, P. D. Maker, R. E. Muller

Jet Propulsion Laboratory, California Institute of Technology, Pasadena, CA 91109

### **Abstract**

The properties of convex gratings fabricated by electron-beam lithography are investigated. Three grating types are shown. The first is a single-panel, true blazed grating in which the blaze angle stays constant relative to the local surface normal. This grating provides high peak efficiency, of approximately 88% in the first order and 85% in the second order. The second grating has two concentric panels, with each panel blazed at a different angle. This type allows flexibility in matching the grating response to a desired form. The third type has a groove shape that departs from the sawtooth blazed profile in order to increase the second order bandwidth. All these types are very difficult or impossible to produce with conventional techniques. The gratings compare favorably with conventional (holographic and ruled) types in terms of efficiency and scatter. Simple scalar models are shown to predict accurately the wavelength response. These gratings allow the optical designer to fully realize the considerable advantages of concentric spectrometer forms.

## 1. Introduction

Spectrometer forms utilizing concentric optical systems<sup>1-4</sup> have been identified as offering a number of advantages.<sup>5</sup> Of the various concentric forms, the Offner spectrometer<sup>6,7</sup> stands out for its compact size, use of only three reflective surfaces, and excellent optical correction. This spectrometer form is very well suited to the requirements of pushbroom imaging spectrometry.<sup>8-12</sup> A typical Offner spectrometer ray trace is shown in Fig. 1. The grating is the aperture stop, and is on the second mirror. The design is telecentric, with a nominal magnification of -1. The primary and tertiary mirrors can sometimes be part of the same curve, but decoupling the two curvatures and separations can be important for good optical correction at low f-numbers. The example shown in Fig. 1 achieves nearly diffraction-limited image quality and submicron distortion over the wavelength band 0.4-1 $\mu$ m, with an f-number of 2.8, slit length of 1.2cm and spectral resolution of 3nm using 12 $\mu$ m square pixels and 1000 spatial pixels. The design utilizes only centered spherical surfaces. Similar performance is possible with designs spanning the range from the uv to the IR up to 12 $\mu$ m. Non-imaging versions, where distortion and large field are not important, can be made extremely compact and match a wide variety of focal plane array formats.

The advantages of the Offner spectrometer form are made possible by the convex grating. Gratings formed on curved (usually concave) substrates are of course not new, and some of their peculiarities have been explored.<sup>13,14</sup> When the curvature of the substrate is significant, it is common practice to change the slope of the diamond cutting tool so as to maintain an approximately constant blaze angle. This results in a multipanel grating (each panel ruled with a fixed tool angle), which typically has a spectral resolution equal to that of one panel since it is not possible to control exactly the phase change between panels<sup>15</sup>. This problem is exacerbated in the Offner design, in which the blaze angle is typically low, on the order of a few degrees, but the curvature of the substrate is considerable. Depending on the f-number of the system, the arc which

the grating must cover is generally more than a few degrees. Thus, the variation in the blaze angle for a fixed ruling tool would be much greater than the blaze angle itself, unless the grating were ruled over several panels.

Holographic gratings do not suffer from this problem, but cannot generally match the efficiency of their ruled counterparts, unless ion-etched to produce a groove profile that approximates that of the ruled grating. However, for the type of grating described above, the direction of the etch must change for nearly every groove, thus adding a significant technical hurdle to this technique.

Electron-beam (E-beam) lithography offers a way of making gratings on such convex substrates that is considerably more flexible than ruling or holographic techniques.<sup>16-18</sup> In this paper, we report experimental results obtained from such gratings, as well as a brief comparison with traditional ruled and holographic gratings. The E-beam technique can produce gratings with no variation in blaze angle across the entire grating surface, independent of substrate convexity up to a certain limit. It also offers the possibility of controlling the shape of the groove in order to achieve a desired diffraction efficiency curve, and to construct multipanel gratings with an arbitrary panel shape, number of grooves, groove spacing etc.

Excimer laser writing or ablation is also a technique that is potentially comparable with E-beam lithography in terms of flexibility.<sup>19,20</sup> However the blazed grating structures reported suffered from groove irregularity that limited the peak efficiency to around 70%.<sup>20</sup>

## **2. Summary of the E-beam fabrication method.**

The method<sup>16-18</sup> involves first coating the flat or low sphericity substrate with a thin (2 – 3  $\mu\text{m}$ ) film of polymethyl methacrylate (PMMA, Plexiglas) using a standard semiconductor fabrication spin-coater. The grating pattern is written by an electron beam lithography tool using, typically, a 50

kV, 2 mA, 0.5  $\mu\text{m}$  waist beam. In order to produce flat, blazed surfaces, it is necessary to compensate for both (a) the nonlinear response of the PMMA and (b) the E-beam 'proximity effect', i.e., exposure produced by electrons that are back-scattered from deep within the substrate. This is accomplished by (a) careful calibration and (b) deconvolution of the experimentally determined delta plus Gaussian instrument function. The exposed patterns are developed in pure acetone for roughly 10 seconds. Final groove depth is adjusted to the design value using incremental development steps interspersed with physical depth measurements. When working with curved substrates, the pattern is subdivided into narrow annular regions that can be exposed adequately at fixed E-beam focal distance. Coincident with changing the focal distance, the E-beam electronic deflector circuits must be adjusted both for scale and rotation. Again careful calibration is necessary. It is found that adequate precision can be realized over a region that varies  $\pm 25 \mu\text{m}$  in height. The equipment and method limitations with respect to total sag have not been investigated, but the maximum surface sag is currently believed to be around 2mm. Figure 2 illustrates the quality of gratings that have been produced using these techniques. It shows atomic force microscope (AFM) data that include the boundary between zones having different blaze angles (see section 5). A fine (sub micron) 'picket fence' of residual PMMA separates the regions. It is the result of imperfect pattern matching and/or exposure.

### **3. Grating specifications and test setup.**

The gratings were produced according to the specifications of the Grating Imaging Spectrometer (GIS) planned for the New Millennium Earth Orbiting 1 (NM-EO1) mission. The GIS is an Offner spectrometer that has a 1cm long slit and operates at an f-number of 7.5 (though the basic design form is compatible with considerably lower f-numbers). It covers the wavelength band of 0.4-2.5 $\mu\text{m}$ , typical of such spectrometers. In order to achieve a compact design the entire wavelength

band is covered by a single spectrometer unit. The grating is thus used in the first (1-2.5 $\mu\text{m}$ ) and second (0.4-1 $\mu\text{m}$ ) orders simultaneously. These wavelength bands and their separation are primarily determined by the spectral response of the focal plane arrays. The two orders are separated with a dichroic mirror; focal plane interference filters further aid in order and background rejection.

Although we are not concerned with the exact design of the GIS spectrometer, its specifications provided a starting point for the design of the gratings reported here; they also serve to show the utility of the gratings in a real application. The basic grating parameters are given in Table 1. Because of the high f-number, it was imperative to achieve high diffraction efficiency over as broad a band as possible.

The grating test setup is shown in Fig. 3. Light from a monochromator slit was input to the Offner spectrometer, which in this case utilized a single mirror in place of separate primary and tertiary. The slit image was recorded on a photodetector, in front of which is an aperture (or slit) slightly larger than the input slit image, so as to exclude light from other orders. Two separate photodetectors were needed in order to cover the entire spectral range: a large-area Si photodiode, and a large-area thermoelectrically cooled PbS detector. Appropriate order-blocking interference filters were also used.

The monochromator (CVI Instruments Digikrom 240) has an f-number of slightly under 7, and an approximately telecentric design, thus matching the Offner spectrometer form. In order to obtain diffraction efficiency measurements, the gratings were replaced by a mirror of the same curvature and coating. Thus the diffraction efficiency curves shown below represent the diffractive properties only, rather than the reflectivity of the coating (relative efficiency).

#### 4. A true blazed grating on a convex substrate.

The first test gratings produced with this technique were true single blaze gratings, in which the blaze angle stays constant with respect to the local grating normal. Such a grating cannot be produced by ruling unless the tool angle is varied continuously for every groove, which is very difficult. For a sawtooth facet profile, the blaze angle  $\theta$  is the angle between the grating normal and the facet normal. It is given by the well-known equation

$$\theta = (\alpha - \beta)/2 \quad (1)$$

where  $\alpha$  and  $\beta$  are the angles of incidence and diffraction respectively. The dependence of  $\theta$  on the angle of incidence means that even with a plane grating incident light must be collimated (constant  $\alpha$ ) in order to have true blazed grating action. With a convex substrate this condition is certainly not satisfied automatically, except that in concentric designs the angle of incidence on the grating typically varies within narrow limits. In this particular case, ray-tracing results revealed a variation in the angle of incidence of less than  $0.7^\circ$  across field and aperture. This greatly simplifies the understanding of the results, since it allows us to simulate the behavior of such gratings through simple planar models.

We present the results from two representative gratings below. The experimental first order diffraction efficiency of the first grating is shown in Fig. 4. As can be seen, the results are very well fitted by a theoretical curve of the form<sup>21,22</sup>

$$D_i = D_{0i} \left[ \frac{\sin(\pi(\frac{\lambda_0}{\lambda} - i))}{\pi(\frac{\lambda_0}{\lambda} - i)} \right]^2 \quad (2)$$

where  $D_i$  is the relative efficiency of the  $i^{\text{th}}$  order,  $D_{0i}$  the corresponding peak efficiency, and  $\lambda_0$  the blaze wavelength in the first order. In fitting this curve, we allow  $\lambda_0$  to vary in order to obtain the best fit. This accounts for experimental uncertainty in the exact value of this wavelength, which is

controlled by the depth of the groove. This uncertainty is typically less than 100nm. We may also note that the above curve is consistent with the rule of thumb that the efficiency of the grating drops to 50% of its peak value at  $\sim 2/3 \lambda_0$  and at  $\sim 9/5 \lambda_0$ .

The second order efficiency of another single blaze grating is shown in figure 5. These results are again fitted with Eq. 2, for  $i = 2$ . The remarkable theoretical fit shown in figures 4 and 5 confirms that the grating behaves as a true single blaze one, and demonstrates the capability of the E-beam technique to manufacture such a grating on a convex substrate.

It was possible to confirm the second order peak efficiency of a single blaze grating using an unexpanded HeNe laser incident on the grating at the angle that maximized the efficiency. Since the second order blaze wavelength is very close to 633nm, the angle of incidence was also close to the one intended for the application. The peak efficiency thus measured was 88%. All gratings tested gave second order efficiencies between the minimum of 81% shown in Fig. 5 and the maximum of 88% obtained with the laser.

## **5. A dual-blaze grating**

The requirements of the NM-EO1 project in terms of broadband response could not be matched by a single blaze grating. Specifically, the second order bandwidth of a single blaze can be seen to be inadequate for the 400-1000nm region (this is inherent in the groove profile rather than an artifact of the method). Also, in the first order, it is required that the response at 2500nm remain as high as possible. But with a single blaze grating it is not possible to push the blaze peak towards longer wavelengths without losing completely the response at the short end, as the curve of fig. 4 demonstrates. To achieve these requirements, the grating area can be split and each region blazed at a different wavelength.

The E-beam technique allows complete flexibility in the design of the area shapes, which is important in certain applications, for example, in controlling the distortion (centroid location) accurately. For this application we chose a grating with two concentric blaze areas. The middle section occupies approximately 33% of the total area and the outer ring the remaining 67%. The two blaze wavelengths were intended to be 1000nm (middle) and 1800nm (ring).

Figure 6 shows the first order efficiency of this grating, and Fig. 7 the second order. The theoretical fits are provided by the equation

$$D = D_{oi} (0.33D_{ai} + 0.67D_{bi}) \quad (3)$$

In this equation, the subscripts a and b stand for the two different blaze areas,  $D$  is the total diffraction efficiency,  $D_{ai}$  and  $D_{bi}$  the first (or second) order efficiencies of the middle and outer sections respectively, as given by Eq. 2 for each order ( $i = 1, 2$ ). Again, the blaze wavelengths were adjusted slightly to account for inaccuracies in the fabrication. The values used were 970nm and 1740nm. The peak efficiency ( $D_0$ ) for each blaze was taken as 88% in the first order and 85% in the second order.

While not perfect, the theoretical fit is still remarkable. This confirms that the two blaze areas can be added incoherently (Eq. 3) for the purpose of measuring diffraction efficiency, and provides a very simple way of designing the response of such gratings (provided the pitch and blaze angle are such that scalar theory suffices). Thus this grating provides a high efficiency over a broad wavelength range.

The E-beam technique provides an additional unique advantage in that it is capable of controlling the average diffracted phase from the different blaze areas. For a ruled grating, the rulings between two different blazes will tend to match at the peaks (Fig. 8(a)). However, with the E-beam technique it is possible to control the average height separately from the groove angle and depth, thus resulting in the profile shown in Fig. 8(b). In this latter case, the mean heights are matched, thus leading to a zero mean phase difference between the two blazes. Of course, such

matching is subject to fabrication error, but the mean phase difference can still be made considerably smaller than would be the case with a ruled grating.

With the grating at the stop, as in the Offner design, any difference in intensity between the two blaze areas represents a pupil apodization, and therefore can have an appreciable effect on the point spread function (PSF), and possibly also on the distortion characteristics which are crucial for imaging spectrometry applications. The effect is further complicated because the mean relative phase of the two areas also enters the calculation. Fourier transformation of the grating profile reveals that for a single blaze area the mean diffracted phase alternates between zero and  $\pi$  whenever the diffraction efficiency goes to zero. If the mean heights of the two blazes are matched exactly, then they add in phase within the area of overlap of the main lobes of the diffraction efficiency curves. This holds in both the first and the second order. If the heights are not exactly matched, then the residual mismatch translates into a phase difference between the two areas, which scales inversely with wavelength.

The following four figures illustrate the procedure. The presentation of these results is easier if we restrict the wavelength range for each order to be the one intended for the NM-EO1 application (1-2.5 $\mu\text{m}$  in the 1<sup>st</sup> order, and 0.4-1 $\mu\text{m}$  in the 2<sup>nd</sup> order).

Two dual blaze gratings were produced. The mean heights were matched within  $\lambda/10$  for the first one, and  $\lambda/5$  for the second ( $\lambda = 632.8\text{nm}$ ). This second grating is the one whose diffraction efficiency was shown in Figs. 6 and 7. In Fig. 9 we show the relative efficiency of each of the two blaze regions separately. These curves are produced using Eq. (2) for each blaze and order, and using the blaze wavelengths identified earlier. The relative phase difference is shown in Fig. 10, for the two actual gratings produced, and also for a grating with a profile corresponding to Fig. 8(a). It is to be noted that this phase difference would be zero for a perfect mean height match. For the grating with the peaks matched (Fig. 8(a)) it can be seen that the phase difference is  $\sim\pi$

over a significant fraction of the wavelength band. This would have a detrimental effect on the PSF.

In the second order, the phase is somewhat more complicated. First, the relative blaze efficiencies are shown in Fig. 11. It can be seen that the efficiency of the second (long  $\lambda$ ) blaze drops to zero at the short wavelengths. Between the two zero crossings it has an average phase of  $\pi$ . This accounts for the discontinuity in the phase difference plot of Fig. 12. In this case, even a perfect mean height match cannot eliminate the phase jump. However, the net effect of this on the PSF is lessened by the fact that the corresponding intensity of the second blaze is low over the region of destructive interference.

The importance of the above discussion is that it provides a model for predicting the effect of the grating blaze areas on the pupil function, in terms of both intensity and phase. This information is critical in determining correctly the PSF and MTF of the spectrometer.

## **6. A dual-angle blazed grating**

The dephasing and apodization problems caused by the two blaze areas are absent in a single blaze design. However, a single blaze design did not have the necessary broad band response, especially in the second order. An alternative way of broadening the second order band is to modify the groove shape away from the sawtooth profile. This will in general reduce the peak efficiency. The profile that was tried is shown in Fig. 13, which justifies the name "dual angle". The flexibility afforded by the E-beam technique in modifying the groove shape to a desired profile should be evident here.

The diffraction efficiency of this grating is shown in Fig. 14. The figure also shows theoretical curves, which were derived from the Fourier transform of the grating profile. Only two free parameters were used for the fitting of both orders simultaneously. The first parameter is the

groove depth, uncertainty in which corresponds to a small fabrication error, as explained previously. This was also used to account for the angle of incidence of the beam. The second parameter is a peak efficiency factor of 0.85, by which both theoretical curves were multiplied so as to match the experimental peak efficiency. It can be seen that the theoretical curves give an excellent fit.

This grating provides an acceptable efficiency down to 400nm, which was impossible to do with the single blaze (compare with Fig. 5). In fact, a slight shift of the blaze peak towards the longer wavelengths would have been possible, as the efficiency below 400nm is expected to show a secondary peak. This would also improve the efficiency around 1000nm. Unfortunately, time and material constraints prevented the fabrication of a second dual-angle grating.

## **7. Other characteristics**

**7.1. Polarization sensitivity.** The gratings were tested in the second order since that is where the polarization is of greatest concern for imaging spectrometry. A high quality sheet polarizer was used in front of the photodetector, but the setup of Fig. 3 was otherwise undisturbed. All gratings tested showed a small sensitivity to polarization in the short wavelength end. The dual blaze grating exhibited about 35% difference between s and p polarizations at 450nm, but considerably less (<10%) over the longer wavelengths. The dual-angle blaze was the most polarization-sensitive of all the gratings due to the finer structure within each groove. The results for this grating are reproduced in Fig. 15.

**7.2. Scatter and Ghosts.** Comparison with ruled and holographic gratings revealed extremely low scatter. These measurements were performed at 632.8nm wavelength, using a focused HeNe laser in place of the input slit, as shown in Fig. 3. A photodetector with a 100 $\mu$ m slit in front of it was used to measure the undesirable light between orders and compare it with the main orders. While

the Offner spectrometer and folding mirrors undoubtedly contributed to scatter, our aim was to compare between the E-beam grating and gratings made through more conventional techniques. Specifically, we had available for comparison both holographic and ruled gratings of the same specifications, the latter being a three-panel design with some inevitable blaze angle variation within each panel.

The scatter (also called "grass") from the E-beam gratings was not measurable with our setup, whereas scatter from both the ruled and holographic gratings was clearly measurable. In the case of the holographic grating, the primary cause of scatter may have been imperfections in the Al coating. Nevertheless, the experimental results were sufficient to show that scatter is of no concern with the E-beam technique. This is also confirmed by the high degree of regularity of the grating grooves as shown in Fig. 2.

The E-beam gratings showed regular ghosts at a spacing equal to one-quarter the spacing between orders. The maximum ghost intensity measured was 0.2% (relative to the second order intensity in HeNe light). These ghosts are caused by the so-called subfield stitching, which is a characteristic of the way the electron beam is scanned in order to cover the entire aperture as the grating is written. There are also some discontinuities over larger areas, called fields, which generate very weak satellites (orders close to the main ones). The intensity of the satellites could not be measured but it was estimated to be at least an order of magnitude smaller than that of the ghosts. However, in both cases the ghosts and satellites were weaker than the equivalent amount of parasitic light generated by the conventional gratings (using the same slit in front of the photodetector), thus demonstrating the high quality of the E-beam gratings.

#### **8. Comparison with a ruled grating.**

In this section we compare briefly the diffraction efficiency of the dual blaze grating with a ruled grating that was manufactured to the same specifications. The ruling was over three panels. A

simple calculation of the blaze angle from Eq. 1, taking into account the angles of incidence and diffraction as well as the substrate convexity, reveals that the blaze wavelength would be expected to vary between 1 and 2.4 $\mu\text{m}$  approximately within each panel, assuming a fixed tool cutting angle for a single panel and appropriate adjustment from one panel to the next. This shows that the substrate convexity is considerable.

The diffraction efficiency comparison is shown in Fig. 16, where we have included both first and second order results for brevity. The exact theoretical treatment of the ruled grating is complicated because it is essentially non-periodic. An incoherent approximation can be obtained using Eqs. (2)-(3), with a large number of partitions. Whether the ruled grating has more than one panel is irrelevant in the sense that the appropriate blaze angles from each of the panels can be taken together. The resulting theoretical curve is shown in Fig. 16. To produce it, it was assumed that the grating was divided into ten different blaze areas with peak blaze wavelengths spanning the range 900-2160nm spaced 140nm apart, each occupying a tenth of the total grating area, and with an arbitrary peak efficiency chosen to match the experimental curve. These parameters are consistent with the expected blaze angle variation across this grating. Inclusion of more wavelengths does not change the result significantly. This simulation is only intended to show that a reasonable approximation to the behavior of a rather complicated diffractive element can be obtained with simple means.

From the comparison it may be seen that the diffraction efficiency of a convex ruled grating can approximate but not match that of an appropriately designed dual panel E-beam grating. With the exception of a small dip in second order efficiency, the E-beam grating efficiency is everywhere higher. Interestingly, for imaging spectrometry applications relying on solar reflected spectrum and a Si-based photodetector, the shape of the second order diffraction efficiency of the dual blaze grating leads to a flat signal-to-noise curve and thus is considered preferable.<sup>6</sup> Different

shapes can of course be obtained by changing the blaze wavelengths and/or the relative blaze areas as desired. This flexibility cannot be matched by either ruled or holographic gratings.

## **9. Conclusions**

The E-beam lithography technique has produced convex gratings that compare favorably with ruled and holographic ones in every respect. In addition, the technique provides significant and often needed flexibility in grating design. True blazed gratings can be produced on curved substrates. More than one blaze areas can be incorporated with equal ease. There is complete flexibility in the shape of these areas, as well as in controlling the mean diffracted phase difference between them. There is also flexibility in modifying the groove shape. The diffraction efficiency of gratings thus produced shows very good agreement with simple scalar models.

Extensions of the techniques are underway in order to increase the permissible sag of the grating substrate, increase the possible groove depth, and reduce the writing time. With these extensions, the technique will be capable of producing gratings for low f-number spectrometers that span the range from the ultraviolet to the thermal infrared. Thus the advantages of concentric spectrometer designs can be fully realized.

## **Acknowledgments**

The research described in this paper was carried out by the Jet Propulsion Laboratory, California Institute of Technology, under a contract with the National Aeronautics and Space Administration. We thank the following JPL colleagues for technical assistance and project leadership: Valerie Duval, Cesar Sepulveda, John J. Simmonds, Christofer Stevens, and David Thomas. The collaboration W. Wong (SSG Inc.) and of Lincoln Labs (MIT) was crucial in securing the ruled and holographic test gratings.

Table 1  
Grating Parameters

Curvature (mm <sup>-1</sup> )	Clear aperture (mm diameter)	Angle of incidence (degrees)	pitch (μm)	λ range 1 <sup>st</sup> order	λ range 2 <sup>nd</sup> order
1.46x10 <sup>-2</sup>	9	~25	20.7	1-2.5 μm	0.4-1 μm

## Figure Captions

Figure 1. A typical Offner spectrometer. The grating is on the convex secondary mirror. The slit is at the top left of the figure, perpendicular to the plane of the paper. The grating grooves are also perpendicular to the paper. The object and image planes are not identical although they are very close in this case. The spectrometer volume (including conjugates) is 14x11x7cm.

Figure 2. AFM scan of typical grating grooves. The blaze angle is only about  $2^\circ$ . It is highly exaggerated for clarity. The picture shows the area around the boundary between two grating sections with different blaze angles. The graph shows the profile of the section marked by a dark line at the bottom right part of the figure.

Figure 3. Schematic of the experimental setup for the evaluation of convex gratings.

Figure 4. Relative diffraction efficiency of a true blazed grating on a convex substrate (first order). The solid curve is derived from equation (2).

Figure 5. Relative diffraction efficiency of a true blazed grating on a convex substrate (second order). The theoretical curve is derived from equation (2) and is chosen to match the experimental points in peak efficiency.

Figure 6. Relative diffraction efficiency of a dual blaze grating in the first order. The theoretical curve is derived from eq. (3).

Figure 7. Relative diffraction efficiency of a dual blaze grating in the second order (same grating as for fig. 6). The theoretical curve is derived from eq. (3).

Figure 8. Profiles of dual blaze gratings. (a) with peaks aligned (b) with equal average heights. In the first case, there is a mean phase difference between the two blaze areas that depends on the height difference  $\Delta h$ .

Figure 9. Relative efficiency of the two blaze areas in the first order. The curves are normalized to unity peak efficiency.

Figure 10. Relative phase difference between the two blaze areas in the first order. The two bottom curves represent the actual gratings manufactured. The topmost curve (triangles) represents a grating with the peaks matched, as in figure 8(a).

Figure 11. Relative efficiency of the two blaze areas in the second order. The curves are normalized to unity peak efficiency.

Figure 12. Relative phase difference between the two blaze areas in the second order. The top two curves shown represent the two dual blaze gratings that were manufactured with approximately matched average heights. The bottom curve (triangles) shows the phase difference for an ideal grating with perfectly matched average heights.

Figure 13. Groove profile of a dual-angle blazed grating. There are two different linear segments. The slopes and groove depth are highly exaggerated for clarity. The actual values for the slopes of the two segments were approximately  $1.5^\circ$  and  $2.8^\circ$ .

Figure 14. Relative diffraction efficiency of a dual angle blazed grating in the first and second orders. The experimental points are shown by the symbols. Squares: first order, triangles: second order. The solid lines show the theoretical fit obtained by a Fourier transformation of the groove profile.

Figure 15. p vs. s efficiency for the dual angle blazed grating in the second order. The average efficiency, as calculated from these two curves, matches the 2<sup>nd</sup> order curve of figure 14 with a few percent error.

Figure 16. Comparison of diffraction efficiencies between a ruled, three-panel grating and a dual blaze E-beam grating. The second order efficiency is shown up to 1000nm, and the first order efficiency beyond that point. Triangles: dual blaze, squares: ruled. A theoretical curve (solid line) to the ruled grating efficiency is also shown.

## References

1. A. Offner: "New concepts in projection mask aligners", *Opt. Eng.* **14**, 130-132 (1975).
2. L. Mertz: "Concentric spectrographs", *Appl. Opt.* **16**, 3122-3124 (1977).
3. J. Dyson: "Unit magnification optical system without Seidel aberrations", *J. Opt. Soc. Am.* **49**, 713-716 (1959).
4. C. G. Wynne: "Monocentric telescopes for microlithography", *Opt. Eng.* **26**, 300-303 (1987).
5. D. R. Lobb: "Theory of concentric designs for grating spectrometers", *Appl. Opt.* **33**, 2648-2658 (1994).
6. F. Reininger et al (46 co-authors): "VIRTIS: Visible infrared thermal imaging spectrometer for the Rosetta mission", in *Imaging Spectrometry II*, SPIE Proc. **2819**, 66-77 (1996).
7. D. R. Lobb: "Imaging spectrometers using concentric optics", in *Imaging Spectrometry III*, SPIE Proc. **3118**, 339-347 (1997).
8. H. H. Zwick: "Evaluation results from a pushbroom imager for remote sensing", *Can. J. Rem. Sens.* **5**, 101-117 (1979)
9. T. J. Brown, F. J. Corbett, T. J. Spera, and T. Andrada: "Thermal infrared pushbroom imagery acquisition and processing" in *Modern Utilization of Infrared Technology VII*, SPIE Proc. **304**, 37-56 (1981).
10. D. J. Diner, C. J. Bruegge, J. V. Martonchik, T. P. Ackerman, R. Davies, S. A. W. Gerstl, H. R. Gordon, P. J. Sellers, J. Clark, J. A. Daniels, E. D. Danielson, V. G. Duval, K. P. Klaasen, G. W. Lilienthal, D. I. Nakamoto, R. J. Pagano, and T. H. Reilly: "MISR: A multiangle imaging spectroradiometer for geophysical and climatological research" *IEEE Trans. Geosci. Rem. Sens.* **27**, 200-214 (1989).

11. P. Silverglate, K. L. Shu, D. Preston, J. Stein, F. Sileo: "Concepts for spaceborne hyperspectral imagery using prism spectrometers" in *Advanced Microdevices and Space Science Sensors*, SPIE Proc. **2267**, 112-120 (1995).
12. O. Saint-Pe, O. Donnadieu, R. Davancens, D. Charlton, A. Menardi, M. Fabbricotti, B. Harnisch, R. Meynart, B. Kunkel: "Development of a 2-D array for 1 to 2.35 $\mu$ m hyperspectral imager" in *Infrared Detectors for Remote Sensing: Physics, Materials, and Devices*, Proc. SPIE **2816**, 138-149 (1997).
13. M. Neviere and W. R. Hunter: "Analysis of the changes in efficiency across the ruled area of a concave diffraction grating", *Appl. Opt.* **19**, 2059-2065 (1980).
14. E. G. Loewen, E. K. Popov, L. V. Tsonev, and J. Hoose: "Experimental study of local and integral efficiency behavior of a concave holographic diffraction grating", *J. Opt. Soc. Am. A* **7**, 1764-1769 (1990).
15. M. C. Hutley: *Diffraction Gratings*, Academic Press (1982).
16. P. D. Maker and R. E. Muller, "Phase holograms in polymethyl methacrylate," *J. Vac. Sci. Technol.*, **10**, 2516-2519 (1992).
17. P. D. Maker and R. E. Muller, "Continuous phase and amplitude holographic elements," U.S. Patent No. 5,393,634, assigned to NASA, issued Feb. 28, 1995.
18. P. D. Maker, D. W. Wilson, and R. E. Muller, "Fabrication and performance of optical interconnect analog phase holograms made by E-beam lithography," in *Optoelectronic Interconnects and Packaging*, R. T. Chen and P. S. Guilfoyle, eds., SPIE Vol. **CR62**, 415-430, (1996).
19. X. Wang, J. R. Leger, and R. H. Rediker: "Rapid fabrication of diffractive optical elements by use of image-based excimer laser ablation" *Appl. Opt.* **36**, 4660-4665 (1997).

20. G. P. Behrmann and M. T. Duignan: "Excimer laser micromachining for rapid fabrication of diffractive optical elements" *Appl. Opt.* **36**, 4666-4674 (1997).
21. D. A. Buralli, G. M. Morris, and J. R. Rogers: "Optical performance of holographic kinoforms", *Appl. Opt.* **28**, 976-983 (1989).
22. H. Dammann: "Blazed synthetic phase only holograms", *Optik* **31**, 95-104 (1970).

**Figure 1**

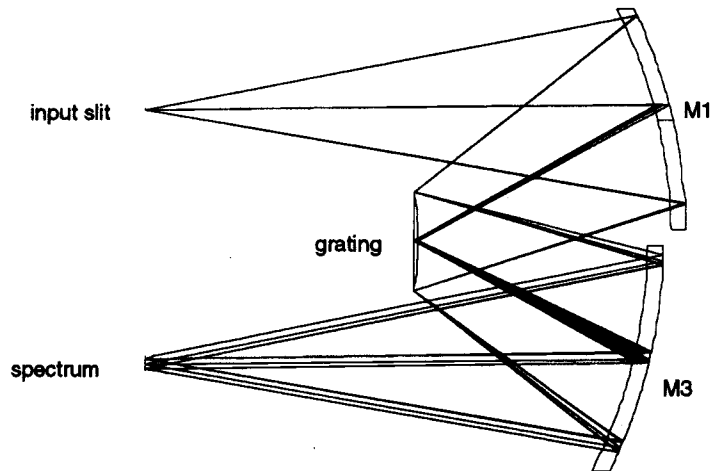
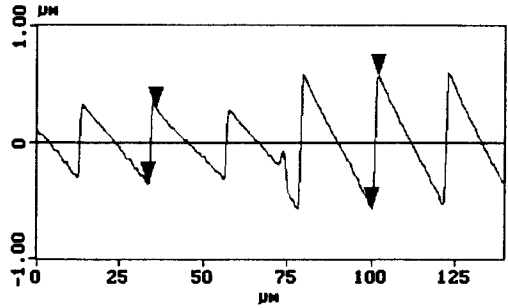
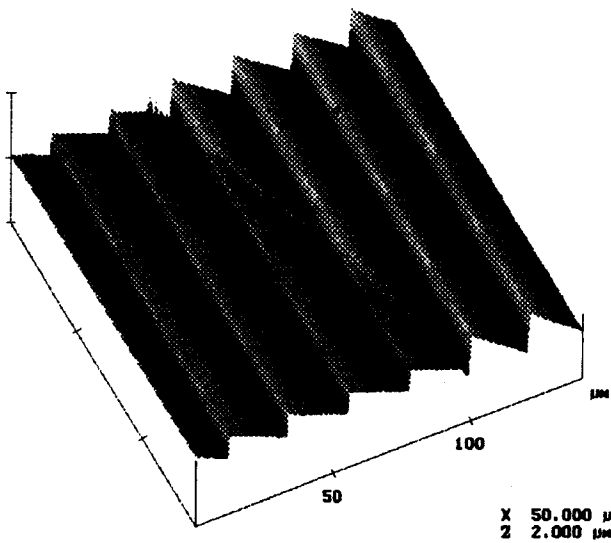


Figure 2



X 50.000  $\mu\text{m}/\text{div}$   
Z 2.000  $\mu\text{m}/\text{div}$

Figure 3

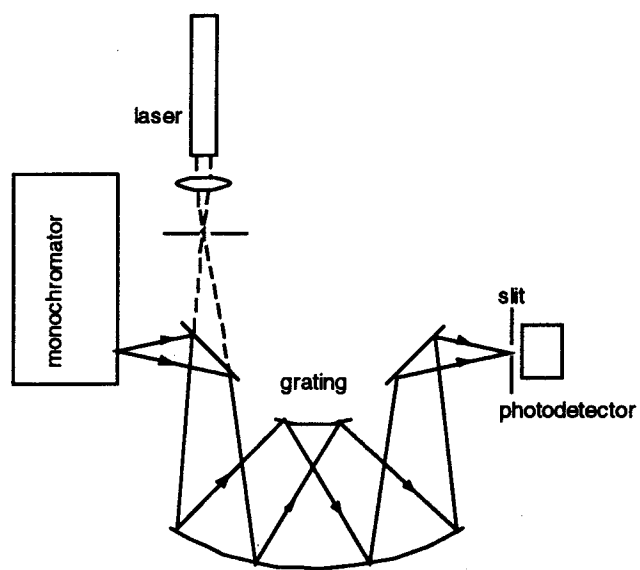


Figure 4

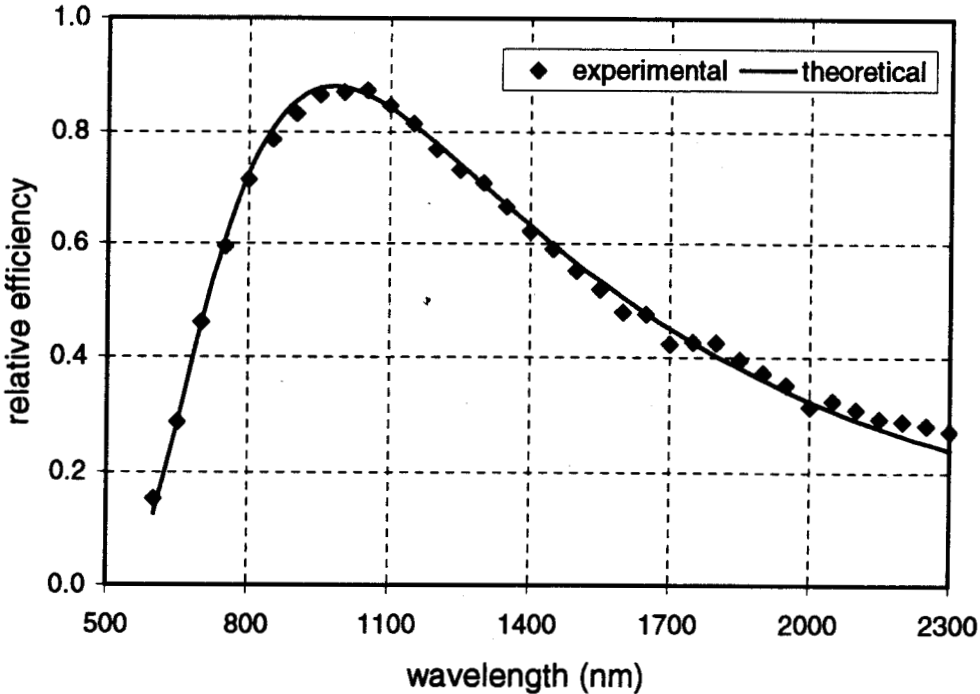


Figure 5

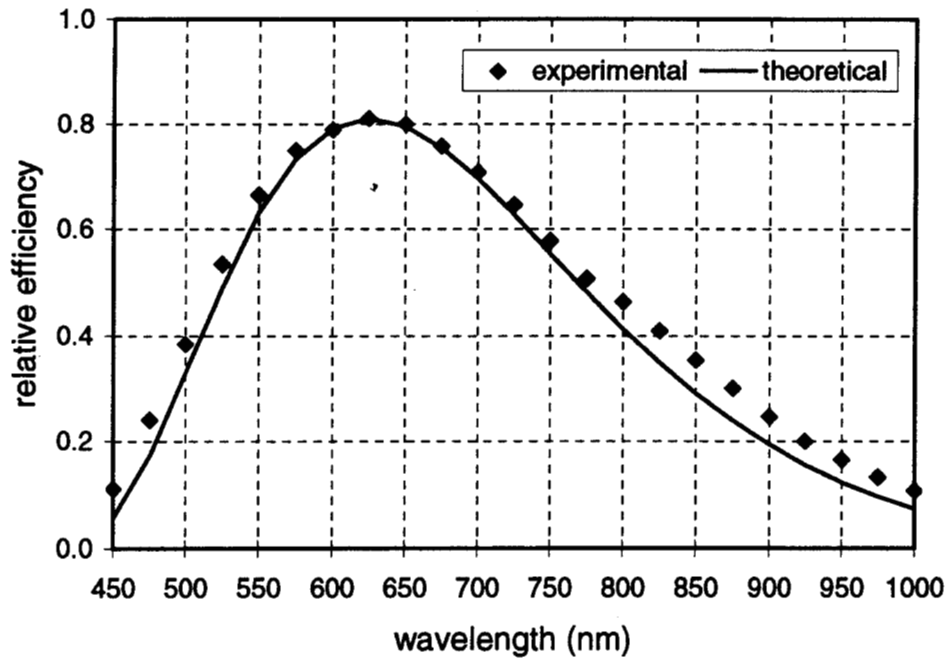


Figure 6

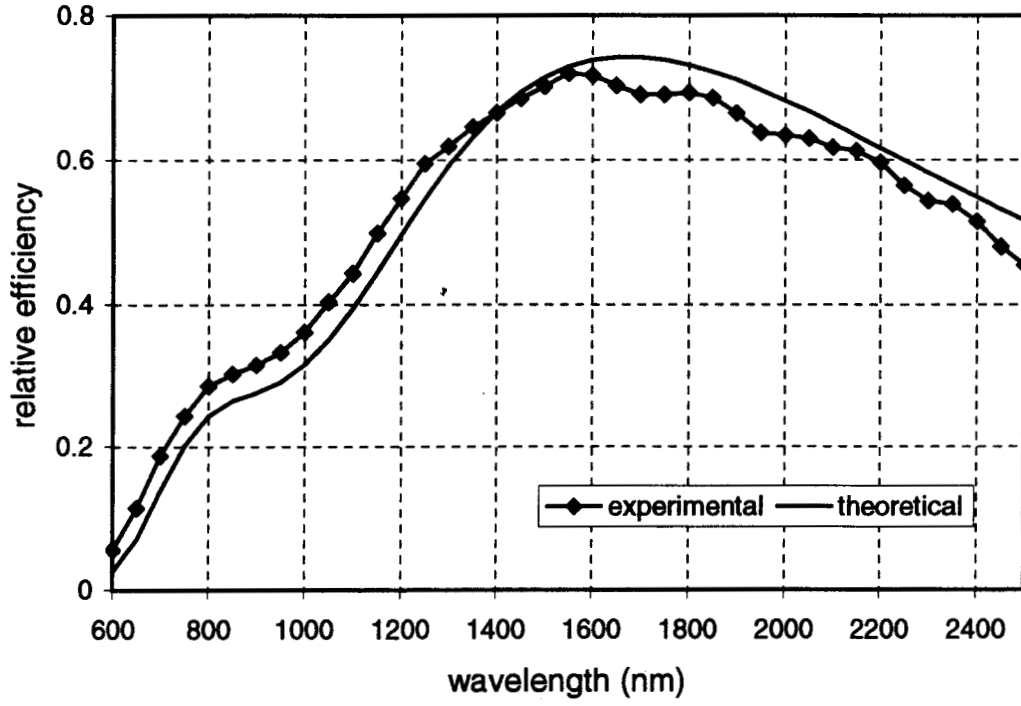


Figure 7

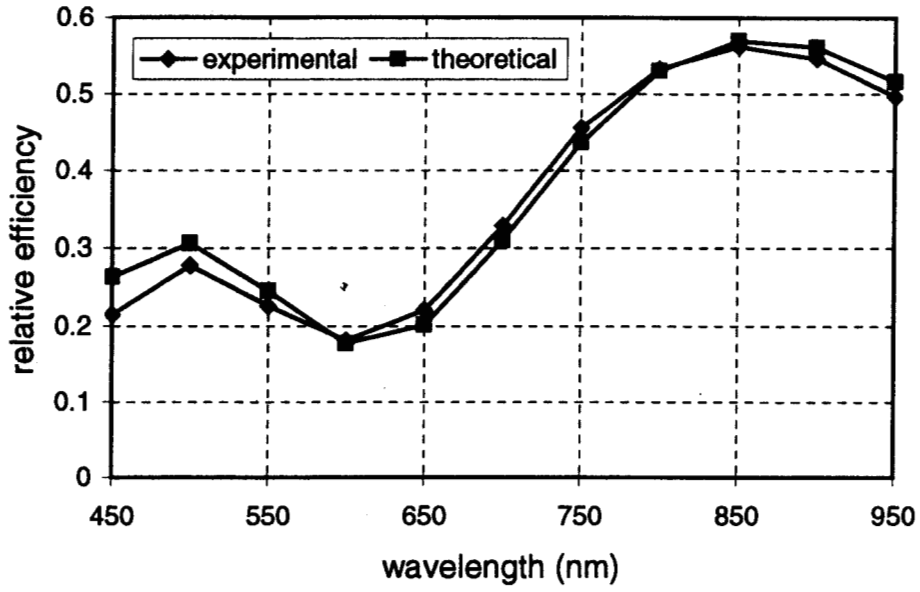


Figure 8

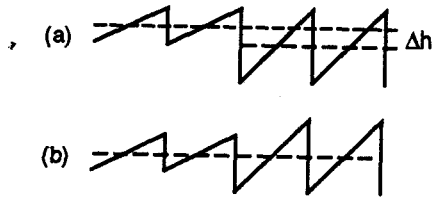


Figure 9

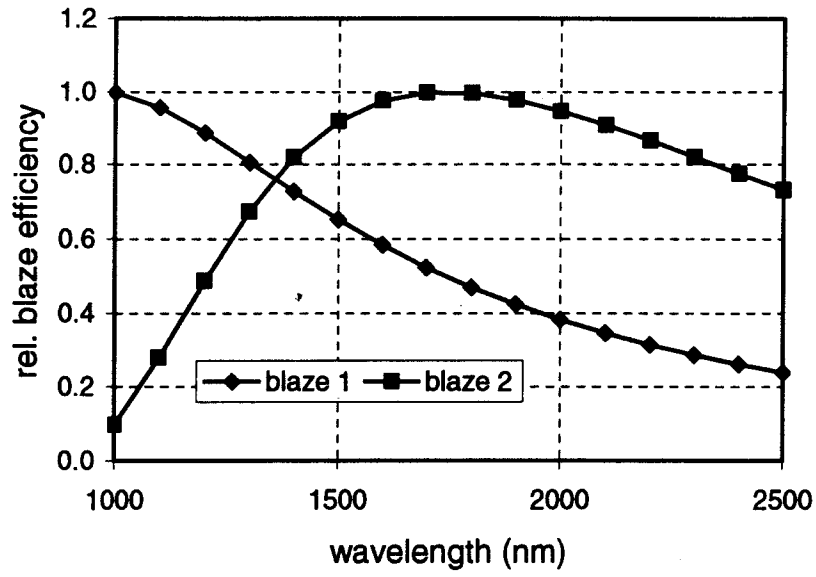


Figure 10

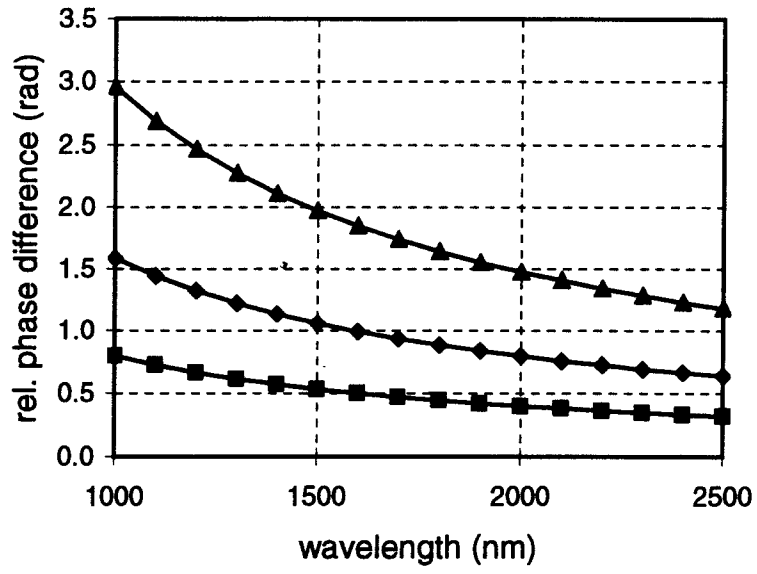


Figure 11

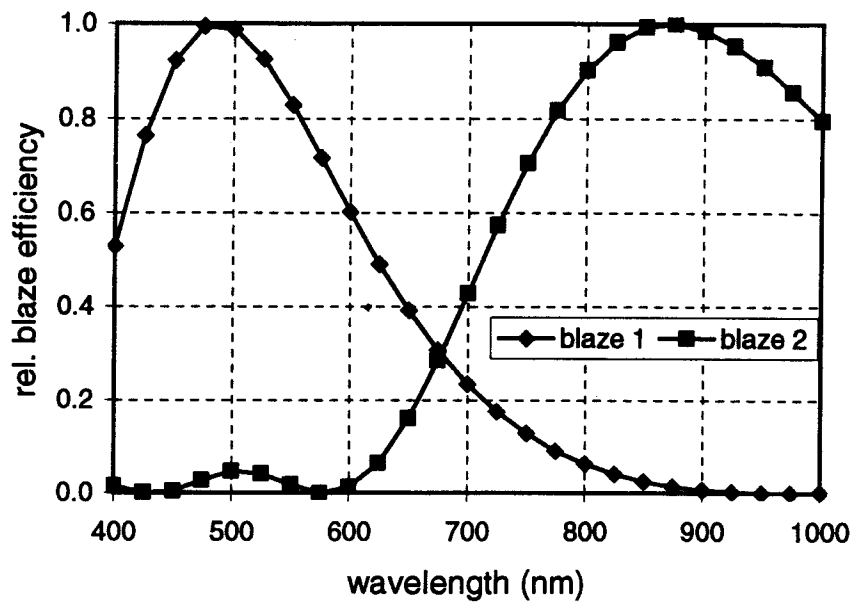


Figure 12

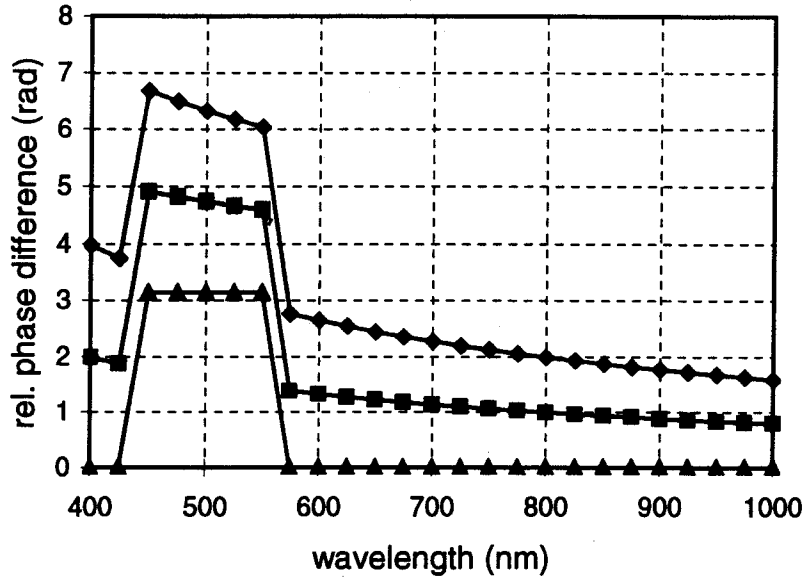


Figure 13

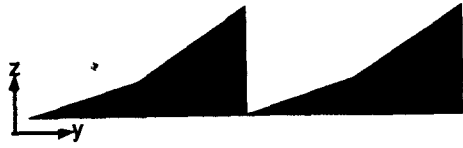


Figure 14

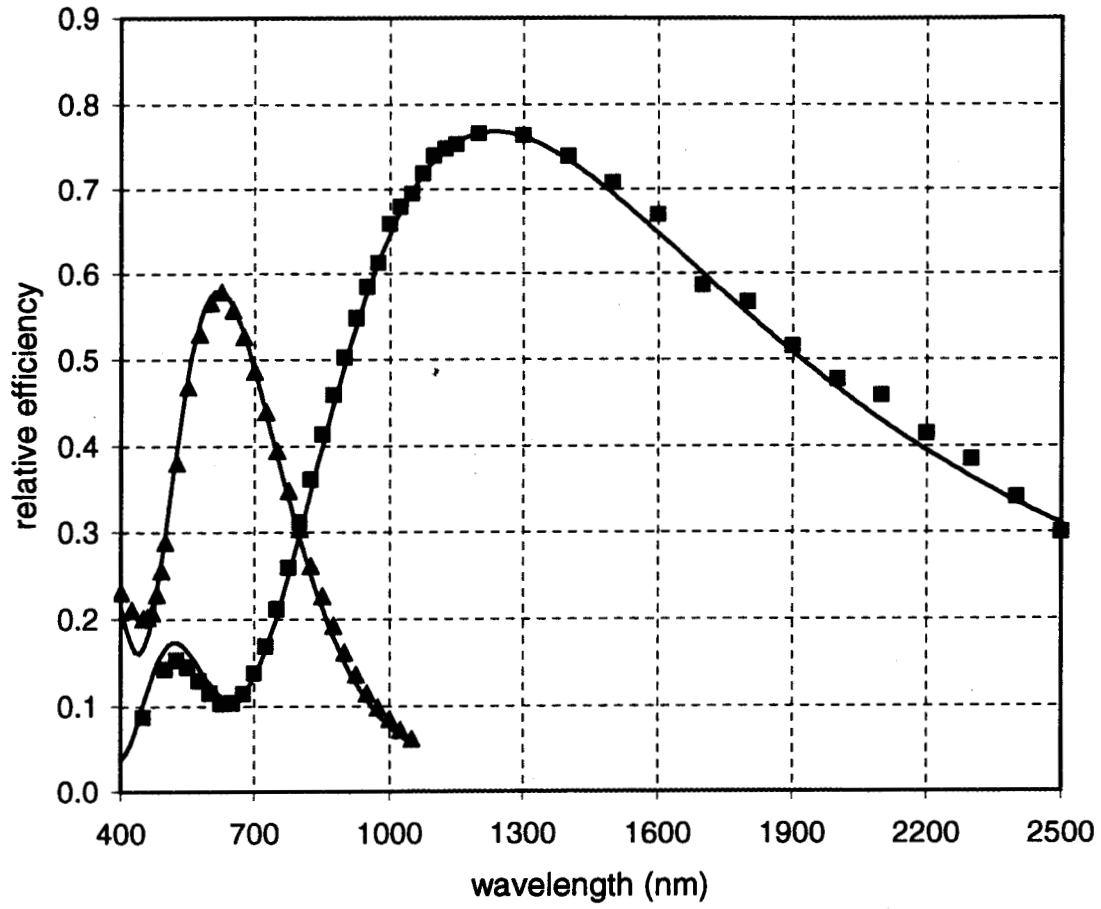


Figure 15

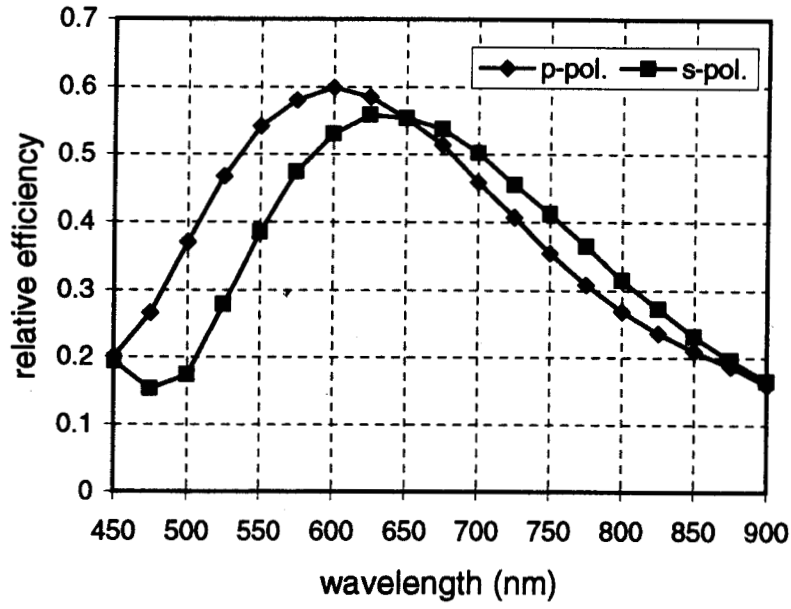


Figure 16

